1-5-2004

Analysis of Microtubule Sliding Patterns in Chlamydomonas Flagellar Axonemes Reveals Dynein Activity on Specific Doublet Microtubules

M. J. Wargo
Dartmouth College

Mark A. McPeek
Dartmouth College

Elizabeth F. Smith
Dartmouth College

Analysis of microtubule sliding patterns in *Chlamydomonas* flagellar axonemes reveals dynein activity on specific doublet microtubules

Matthew J. Wargo, Mark A. McPeek and Elizabeth F. Smith*

Department of Biological Sciences, Dartmouth College, Hanover, NH 03755, USA

*Author for correspondence (e-mail: elizabeth.f.smith@dartmouth.edu)

Accepted 5 January 2004
Journal of Cell Science 117, 2533-2544 Published by The Company of Biologists 2004
doi:10.1242/jcs.01082

Summary

Generating the complex waveforms characteristic of beating eukaryotic cilia and flagella requires spatial regulation of dynein-driven microtubule sliding. To generate bending, one prediction is that dynein arms alternate between active and inactive forms on specific subsets of doublet microtubules. Using an in vitro microtubule sliding assay combined with a structural approach, we determined that ATP induces sliding between specific subsets of doublet microtubules, apparently capturing one phase of the beat cycle. These studies were also conducted using high Ca^{2+} conditions. In *Chlamydomonas*, high Ca^{2+} induces changes in waveform which are predicted to result from regulating dynein activity on specific microtubules. Our results demonstrate that microtubule sliding in high Ca^{2+} buffer is also induced by dynein arms on specific doublets. However, the pattern of microtubule sliding in high Ca^{2+} buffer significantly differs from that in low Ca^{2+}. These results are consistent with a 'switching hypothesis' of axonemal bending and provide evidence to indicate that Ca^{2+} control of waveform includes modulation of the pattern of microtubule sliding between specific doublets. In addition, analysis of microtubule sliding in mutant axonemes reveals that the control mechanism is disrupted in some mutants.

Key words: Flagella, Microtubule, Dynein, *Chlamydomonas*

Introduction

Our current understanding of ciliary and flagellar bending is founded on a dynein-driven microtubule sliding mechanism (Brokaw, 1989; Satir, 1968; Shingyoji et al., 1977). Axonemal dyneins generate force in a single direction (Fox and Sale, 1987; Sale and Satir, 1977). Thus, producing the complex waveforms characteristic of beating cilia and flagella requires that dynein activity is regulated; at any single moment during beating, dynein arms on only a subset of doublet microtubules are active. Based on this model, one prediction is that dynein arms switch between active and inactive forms on specific subsets of doublet microtubules to generate principal and reverse bends. Genetic and functional analyses indicate that simple oscillatory bending is a feature of the dynein arms, outer doublets, and a feedback system that controls microtubule sliding (Kamiya, 2002). Several studies have contributed to a model in which the asymmetry of the central apparatus plays a role in modulating the switch-point to activate sliding on specific microtubules (reviewed by Satir, 1985) (see also Lindemann, 2003; Wargo and Smith, 2003).

The use of isolated axonemes in an in vitro microtubule sliding assay provides a unique opportunity to test this model and examine the possible role of the central apparatus in modulating dynein activity on specific doublet microtubules (Nakano et al., 2003; Wargo and Smith, 2003; Yoshimura and Shingyoji, 1999). In the sliding assay, the addition of ATP and protease to isolated axonemes uncouples axonemal bending from dynein-driven microtubule sliding between adjacent doublets (Okagaki and Kamiya, 1986; Summers and Gibbons, 1971). By combining this functional assay with a structural approach, the identities of the doublet microtubules with active dynein arms can be deduced, and the orientation of the central apparatus relative to active microtubule sliding determined. This approach has been used to successfully investigate dynein arm activity in cilia and flagella for several organisms including echinoderm sperm flagella (Mohri et al., 1987; Nakano et al., 2003; Sale, 1986) and mussel cilia (Satir and Matsuoka, 1989). In cilia and flagella from these organisms, the central apparatus maintains a fixed orientation relative to the plane of beating and thus, relative to the position of active microtubule sliding.

For some organisms, such as *Paramecium* and *Chlamydomonas*, the central apparatus rotates during beating (Omoto et al., 1999). In these cilia and flagella the relationship of central apparatus asymmetry to active microtubule sliding is less well defined. We recently used electron microscopy to determine the orientation of the central apparatus in flagellar axonemes isolated from *Chlamydomonas* cells following the induction of microtubule sliding. Our analyses revealed that the C1 microtubule of the central apparatus is oriented towards the region of active microtubule sliding (Wargo and Smith, 2003). These results provided structural evidence that the asymmetry of the central apparatus correlates with the location of dynein-driven microtubule sliding, most likely through interactions with the radial spokes.

Using the same functional approach combined with structural markers that distinguish the outer doublet microtubules (Hoops and Witman, 1983) we have now assessed whether dynein-driven microtubule sliding occurs

between specific subsets of doublet microtubules. In addition, we have assessed whether changes in Ca^{2+} concentration modulate this activity. In low Ca^{2+} conditions (pCa<8) *Chlamydomonas* flagella beat with an asymmetric waveform; when intraflagellar Ca^{2+} concentration increases to pCa4, the flagella beat with a symmetric waveform (Bessen et al., 1980; Hyams and Borisy, 1978; Omoto and Brokaw, 1985). Changing waveform is predicted to result from modulation of dynein activity on specific doublet microtubules. We hypothesized that these regulatory changes would be detected as a change in dynein activity on specific subsets of doublets.

Using a microtubule sliding assay, we discovered that microtubule sliding occurs between specific subsets of microtubules in wild-type axonemes in both low and high Ca^{2+} conditions. In both Ca^{2+} conditions the assay appears to capture the sliding of microtubules predicted to drive the effective stroke. In addition, the patterns of microtubule sliding produced in high Ca^{2+} conditions differ significantly from those in low Ca^{2+} conditions. Also, compared to wild-type axonemes, the pattern of microtubule sliding in some mutant axonemes was altered and defective in response to changes in Ca^{2+}. These results demonstrate that subsets of outer doublet microtubules are selectively extruded following ATP-induced microtubule sliding in *Chlamydomonas* axonemes and are consistent with a 'switching hypothesis' of axonemal bending. In addition, these results support the hypothesis that Ca^{2+}-induced changes in waveform affect dynein activity on specific doublet microtubules to alter the pattern of microtubule sliding.

Materials and Methods

Chlamydomonas strains and cell culture

Chlamydomonas reinhardtii strain A54-e18 (*nit1-1, ac17, sr1*, mt+) was obtained from Paul Lefebvre (University of Minnesota, St Paul, MN, USA), the *cpc1-2* strain from David Mitchell (SUNY, Syracuse, NY, USA) and the *pf30pf28* strain from Winfield Sale (Emory University, Atlanta GA, USA). The strains 137c, *pf3*, *pf6*, *pf14*, *pf17*, *pf28*, *oda1* and *ida1* were obtained from the *Chlamydomonas* Genetics Center (Duke University). Cells were grown in constant light in TAP medium (Gorman and Levine, 1965). *Chlamydomonas* strains cited in the text are listed in Table 1.

Axoneme isolation and the microtubule sliding assay

Flagella were severed from cell bodies by the dibucaine method (Witman, 1986) and isolated by differential centrifugation in buffer A (10 mM Hepes, pH 7.4, 5 mM $MgSO_4$, 1 mM DTT, 0.5 mM EDTA and 50 mM potassium acetate). Axonemes were isolated by adding NP-40 (Calbiochem, La Jolla, CA) to flagella for a final concentration of 0.5% (wt/vol) to remove membranes. The axonemes were pelleted, resuspended in buffer A, and immediately prepared for the microtubule sliding assay.

The microtubule sliding assay was based on previously described methods (Okagaki and Kamiya, 1986; Summers and Gibbons, 1971). For analysis of cross sections, axonemes were pelleted and resuspended in reactivation buffer (buffer A, 1 mM ATP). An equal volume of sliding buffer (buffer A, 1 mM ATP, 4 μg/ml protease) was added to the axonemes and thoroughly mixed. We used either Nagarse protease (Type XXVII protease; Sigma Chemical Co., St Louis, MO) or Type VIII protease (catalogue number P-5380, Sigma). Both proteases produced the same results. For Ca^{2+} treatments, buffer A, the reactivation buffer, and the sliding buffer included $CaCl_2$ for a final concentration of 10^{-4} M free Ca^{2+}. Sliding was monitored by darkfield microscopy (Smith, 2002b). Exactly 3 minutes after the addition of sliding buffer, 8% glutaraldehyde was added to the sample for a final concentration of 1%, and the sample was processed for electron microscopy (Wargo and Smith, 2003).

Electron microscopy

Axonemes were pelleted and fixed in 1% glutaraldehyde and 1% tannic acid in 0.1 M sodium cacodylate for 1 hour, and post-fixed in 1% osmium tetroxide. The samples were stained with 1% aqueous uranyl acetate, dehydrated in a graded series of ethanol and embedded in EMbed-812 resin. Uniform gold-silver sections were mounted on copper grids, stained with uranyl acetate and Reynold's lead citrate, and examined in a JEOL 100CX, JEOL 2000FX or JEOL 1010 transmission electron microscope. Glutaraldehyde, osmium tetroxide, tannic acid, sodium cacodylate, lead nitrate and copper grids were purchased from EM Sciences (Fort Washington, PA, USA). For data analysis, negatives were digitized using an optical scanner.

Statistical analysis of images

In transverse sections, axonemes lacking doublet microtubules were considered to be those in which active microtubule sliding had occurred following the addition of ATP and protease. All images were oriented with the dynein arms projecting clockwise, the axoneme viewed proximal to distal (Fig. 1A). Transverse sections of axonemes revealed one of six different sliding patterns (Fig. 1B). For each sliding pattern, the axoneme was partitioned into active and inactive areas. The active area is the region in which dynein-driven microtubule sliding resulted in the loss of doublet microtubules from the remainder of the axoneme; this area includes the exposed A-tubule and dynein arms and extends to the exposed B-tubule (Fig. 1). The inactive area includes the remainder of the axoneme.

Two types of analyses are plotted in the figures. First, for sliding pattern data the percentage of transverse sections showing each of six possible sliding patterns (Fig. 1B) was determined for each independent experiment. The number of events (the number of transverse sections examined) and the number of independent trials are specified in the appropriate figure legends. The sliding pattern histograms were constructed by calculating the mean of the percentage contribution of each pattern from all trials. Second, for data regarding the identity of the outer doublet on the dynein exposed edge of the active area, doublet number was determined according to the criteria of Hoops and Witman (Hoops and Witman, 1983). The key identifying structure was the lack of an outer dynein arm on doublet one and the unusual cross-bridge between doublets one and two (Fig. 1A).

We analyzed the sliding pattern data and outer doublet identity data using chi-squared goodness of fit tests (Sokal and Rohlf, 1995). Our expectation was that events would be uniformly distributed among all categories. For sliding pattern data, this means that each of the six sliding pattern categories is expected to contain 16.67% (1/6) of the total events. For the outer doublet identity data, each doublet category would be expected to contain 11.11% (1/9) of events based on nine possible outer doublet microtubules.

Sliding patterns and doublet number data were also characterized for a number of mutant and wild-type strains. These experiments produced large and complex data sets for multiple strains and different Ca^{2+} conditions. To quantitatively compare similarities and differences among all strains and conditions analyzed, we utilized principal components (PCs) analyses (Morrison, 1990). PCs analysis reduces the number of variables in a data set to a smaller number of newly derived variables (the principal components) that summarize the greatest sources of information contained in the original variable set. Reducing the variable set allows for easier comparison among multiple samples (in this case cell strains and different Ca^{2+} conditions) and multiple variables (in this case microtubule sliding patterns or outer doublet identity). The newly derived variables are

extracted so that the first principal component explains the greatest amount of the variance in the original data set; the second principal component explains the second greatest amount of variance, and so forth (Morrison, 1990). Therefore, for the data presented here the principal components summarize the major patterns of variation among axonemes isolated from several strains and induced to slide in conditions of low and high Ca^{2+} buffer. Separate PCs analyses were performed for microtubule sliding pattern data and doublet number data. Since all variables were measured in the same units, and differences in variance significantly contribute to interpretation, principal components were extracted from covariance matrices (Morrison, 1990). PCs analyses were performed using PC-SAS version 8.02 (SAS Institute, Inc. 2001. SAS/STAT User's Guide, Version 8.02, Volume 2. Cary, North Carolina).

Results

Dynein arms on specific doublets induce microtubule sliding

We used an in vitro sliding assay followed by electron microscopy to determine if dynein arms on specific subsets of doublet microtubules are active. By adding ATP and protease to isolated axonemes, dynein-driven microtubule sliding results in the loss of doublet microtubules from the axonemes. We then examined transverse sections of axonemes following ATP-induced microtubule sliding using electron microscopy. The portion of the axoneme that lacked doublet microtubules was defined as the location of active sliding (Fig. 1A) (see also Wargo and Smith, 2003).

We first analyzed the distribution of microtubule sliding patterns resulting from ATP-induced activation. A transverse section of a wild-type axoneme following microtubule sliding is shown in Fig. 1A. Every transverse section in which the doublet microtubules remained associated with the central pair and the number of associated doublet microtubules could be determined was categorized as one of six possible sliding patterns, depending on the number of doublets remaining associated with the central pair (Fig. 1B).

The sliding patterns of two *Chlamydomonas* strains that are wild-type for motility (A54-e18 and 137c) were first examined in low Ca^{2+} conditions (Fig. 2A). Notably, for both wild-type strains, the P8 and P7 sliding patterns were most prevalent. If microtubule sliding occurred randomly between doublet microtubules, we expected a uniform distribution of the six possible sliding patterns in the transverse sections examined. For both wild-type strains the distribution was not random (A54-e18: χ^2=21.81, df=5, P<0.001; 137c: χ^2=81.34, df=5, P<0.001). The two strains do differ quantitatively in the relative frequencies of the various sliding patterns (χ^2=16.12, df=1, P<0.001); however, the qualitative patterns are similar in that the P8 pattern, in which only one outer doublet slid away from the axoneme, was most commonly observed, followed by the P7 pattern (Fig. 2A).

We also determined whether active sliding occurs between specific subsets of doublet microtubules. Structural analyses performed by Hoops and Witman (Hoops and Witman, 1983) revealed several structural asymmetries in *Chlamydomonas* axonemes. Most relevant to our study, a single doublet microtubule lacks outer dynein arms along the entire length of the axoneme (Hoops and Witman, 1983). This microtubule was designated doublet number one (Db1, Fig. 1A); the remaining microtubules were numbered consecutively in the clockwise direction, viewing the axoneme from proximal to distal (Fig. 1A). Db1 of each flagellum faces the other flagellum; therefore, for both flagella Db1 is always on the outside edge of the principal bend of the effective stroke (Fig. 1C). Using this reference system, we determined the identities of the doublet microtubules that remained associated with the central pair following the induction of microtubule sliding. Db1 was

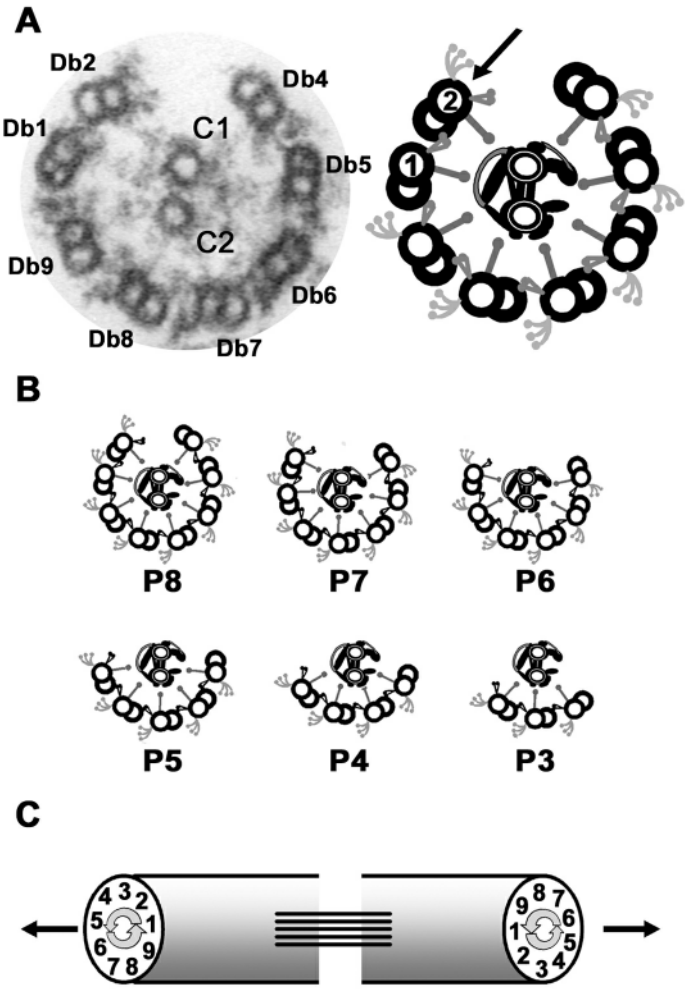

Fig. 1. (A) Electron micrograph and accompanying diagram of axonemal transverse section following the induction of microtubule sliding. The axoneme is oriented as viewed, proximal to distal and based on the doublet (Db) numbering system of Hoops and Witman (Hoops and Witman, 1983). Db3 has slid away from the axoneme leaving doublet 2 on the dynein exposed edge of the active area (arrow). (B) Diagram of the six possible sliding patterns observed following ATP-induced microtubule sliding. The associated central apparatuses are not meant to imply that only transverse sections with a specific central apparatus orientation are included in the analysis. The numbers indicate the number of doublet microtubules that remain associated with the central apparatus. (C) Flagella as viewed looking towards the cell body. The arrows indicate the direction of the beat plane during the effective stroke.

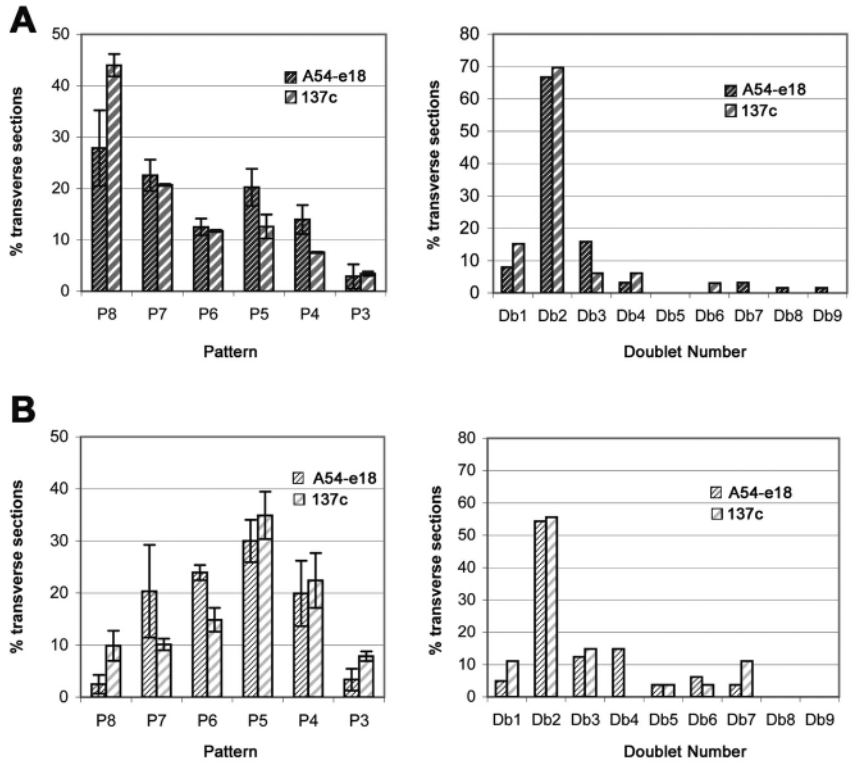

Fig. 2. (A) Distributions of the microtubule sliding patterns (Pattern) and the doublet present at the dynein-exposed edge of the active area (Doublet Number) following the induction of microtubule sliding in low Ca^{2+} buffer. For sliding pattern data, A54-e18: 3 trials, *n*=110. 137c: 3 trials, *n*=145. For doublet number data: A54-e18: 3 trials, *n*=63. 137c: 3 trials, *n*=33. (B) Distributions of the microtubule sliding patterns (Pattern) and the doublet present at the dynein-exposed edge of the active area (Doublet Number) following the induction of microtubule sliding in high Ca^{2+} buffer. For sliding pattern data: A54-e18: 3 trials, *n*=171; 137c: 3 trials, *n*=90. For doublet number data: A54-e18: 3 trials, *n*=81; 137c: 3 trials, *n*=27.

identifiable in 25-60% of transverse sections depending on the strain. Since the number of microtubules that have slid away from the remainder of the axoneme also varied for different strains, this data is presented graphically as the identity of the outer doublet present at the dynein-exposed edge of the active area (arrow, Fig. 1A).

Db2 is present at the dynein-exposed edge of the active area in greater than 60% of wild-type axonemes (A54-e18 and 137c) in which sliding occurred in low Ca^{2+} buffer (right panel, Fig. 2A). This observation combined with a predominantly P8 or P7 sliding pattern indicates that Db3 and Db4 are most often absent from transverse sections of wild-type axonemes following the induction of microtubule sliding. Therefore, in low Ca^{2+} conditions the dynein arms on Db2, Db3, and/or Db4 are the predominantly active dynein arms.

Microtubule sliding patterns are altered by Ca^{2+}

If Ca^{2+}-induced changes in waveform result from modulating dynein activity on specific subsets of doublet microtubules, we hypothesized that these regulatory changes would be detected as changes in the pattern or position of microtubule sliding in the in vitro assay. Analysis of microtubule sliding patterns in high Ca^{2+} conditions revealed that the distributions of sliding patterns for both wild-type strains (A54-e18 and 137c, Fig. 2B) were significantly different from those observed in low Ca^{2+} buffer, with the P4 and P5 sliding patterns predominating (χ^2=55.73, df=1, *P*<0.001; compare left panels of Fig. 2A and B). In these high Ca^{2+} conditions, microtubule sliding was also not random for either strain (A54-e18: χ^2=81.43, df=5, *P*<0.001; 137c: χ^2=29.77, df=5, *P*<0.001). Again, the two wild-type strains differed quantitatively from one another in the frequencies of the various sliding categories (χ^2=8.78, df=1, *P*<0.003), but their qualitative patterns were similar, with the P5 pattern predominating and with substantial numbers of P6 and P4 patterns as well (Fig. 2B, left panel).

We also determined the identities of the doublet microtubules observed in transverse section following the induction of microtubule sliding as described above (Fig. 2, right panels). In high Ca^{2+} buffer, Db2 is at the dynein-exposed edge of the active area in greater than 50% of transverse sections of slid wild-type axonemes (A54-e18 and 137c, Fig. 2B, right panel). This result combined with the observation that induction of microtubule sliding in high Ca^{2+} buffer predominantly results in a P5 sliding pattern indicates that doublets Db3, Db4, Db5 and Db6 are most often absent in transverse sections of wild-type axonemes following sliding. Therefore, in high Ca^{2+} conditions the active dynein arms may include those on Db2-Db6. However, shearing most commonly occurred between Db2 and Db3.

Analysis of mutant strains in low and high Ca^{2+} conditions

Numerous studies support a model in which the central apparatus and radial spokes function as a control system to modulate dynein activity, and include a possible role in Ca^{2+} control of waveform (reviewed by Porter and Sale, 2002) (see also Yang and Sale, 2001; Smith, 2002b). While the precise role of the radial spoke-central apparatus control system in modulating motility has yet to be determined, the ultimate target of the control system is predicted to be the dynein arms on specific subsets of microtubules. In addition, regulation of motility may involve specific dynein subforms and the dynein regulatory complex.

To test this prediction, we analyzed microtubule sliding in

Table 1. *Chlamydomonas* strains used in this study

Strain	Structural/motility defect
A54-e18	no axonemal structural defect/wild-type motility (Smith and Lefebvre, 1996)
137c	no axonemal structural defect/wild-type motility (Harris, 1989)
oda1, pf28	lack outer dynein arms/flagella beat with one-half frequency (Kamiya and Okamoto, 1985; Mitchell and Rosenbaum, 1985)
ida1, pf30	lacks inner dynein arm subform I1/ reduced beat frequency, altered waveform (Brokaw and Kamiya, 1987)
pf30pf28	lacks outer dynein arms and inner dynein arm I1 (Piperno et al., 1990; Smith and Sale, 1992)
pf3	defects in dynein regulatory complex/reduced beat frequency, altered waveform (Brokaw and Kamiya, 1987; Kamiya et al., 1991; Piperno et al., 1992)
pf6	central apparatus, lacks 1A projection/flagella paralyzed or twitch (Dutcher et al., 1984)
cpc1	central apparatus, lacks 1B projection/reduced beat frequency (Mitchell and Sale, 1999)
pf14	lacks radial spokes/paralyzed flagella (Piperno et al., 1977)
pf17	lacks radial spoke heads/paralyzed flagella (Huang et al., 1981)

both low and high Ca^{2+} conditions for axonemes isolated from mutants with defects in the radial spokes, central apparatus, dynein arms, or dynein regulatory complex components. The mutants and their corresponding structural defects are listed in Table 1. The frequencies of both the microtubule sliding pattern and the identity of the outer doublet microtubule on the dynein exposed edge of the active area for central apparatus defective and radial spoke defective strains are shown in Fig. 3; the sliding pattern and outer doublet identity frequencies for dynein arm and dynein regulatory complex-defective strains are shown in Fig. 4.

Initial inspection of microtubule sliding patterns revealed two trends: microtubules of mutant axonemes appeared to slide with either a P7/P8 pattern or a P5/P6 pattern regardless of Ca^{2+} condition (compare left panels, Figs 3 and 4). In addition, while induction of microtubule sliding in several mutants resulted in Db2 on the dynein exposed edge of the active area, several mutants displayed considerable variation in terms of which doublet was present on the dynein exposed edge.

To quantitatively compare the results for all strains examined, these data were analyzed using principal components (PCs) analysis. PCs analysis allows for the quantitative comparison of complex data sets that include multiple samples (in this case, cell strains and different Ca^{2+} conditions) with multiple variables (in this case, microtubule sliding patterns or outer doublet identity). Essentially, the number of variables is reduced to a smaller number of newly derived variables (the principal components) that effectively summarize information contained in the original variable set. In this study, the principal components summarize the major patterns of variation among axonemes isolated from multiple strains and induced to slide in

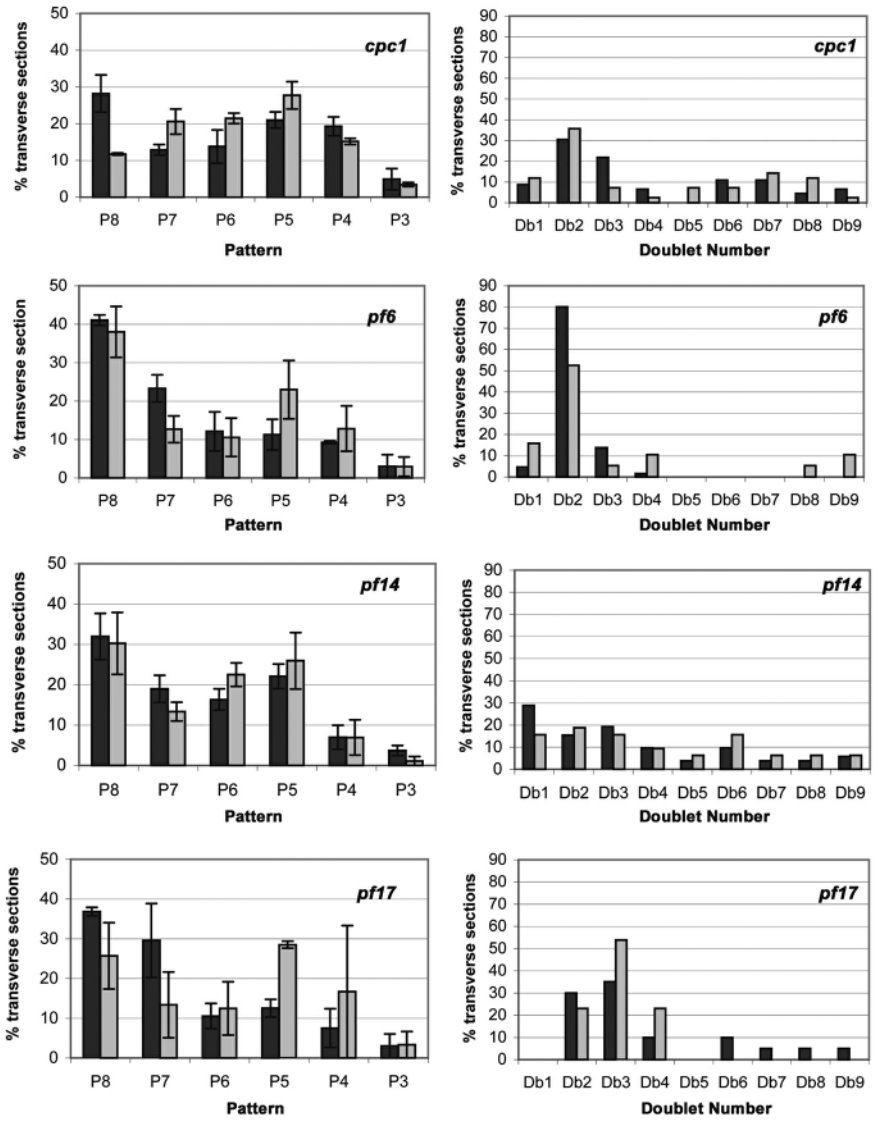

Fig. 3. Distributions of the microtubule sliding patterns (Pattern) and the doublet present at the dynein-exposed edge of the active area (Doublet Number) following the induction of microtubule sliding in low (dark bars) and high (light bars) Ca^{2+} buffer. For microtubule sliding pattern data: *cpc1* low Ca^{2+}: 3 trials, n=143; high Ca^{2+}: 3 trials, n=84; *pf6* low Ca^{2+}: 3 trials, n=125; high Ca^{2+}: 4 trials, n=90; *pf14* low Ca^{2+}: 4 trials, n=105; high Ca^{2+}: 4 trials, n=95; *pf17* low Ca^{2+}: 3 trials, n=64; high Ca^{2+}: 3 trials, n=50. For doublet number data: *cpc1* low Ca^{2+}: 3 trials, n=46; high Ca^{2+}: 3 trials, n=42; *pf6* low Ca^{2+}: 3 trials, n=65; high Ca^{2+}: 3 trials, n=19; *pf14* low Ca^{2+}: 4 trials, n=52; high Ca^{2+}: 4 trials, n=32; *pf17* low Ca^{2+}: 3 trials, n=20; high Ca^{2+}: 3 trials, n=13.

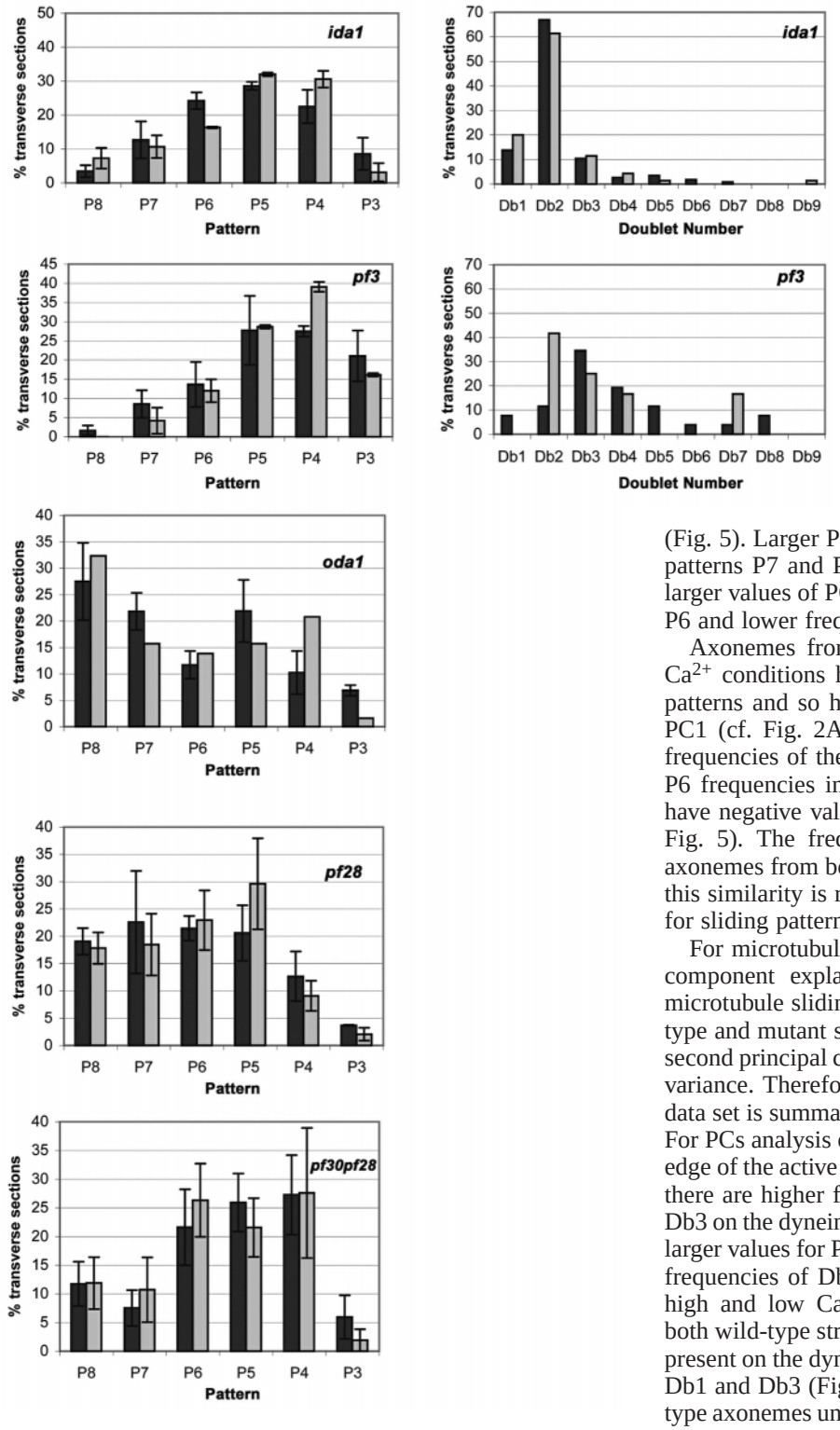

Fig. 4. Distributions of the microtubule sliding patterns (Pattern) and the doublet present at the dynein-exposed edge of the active area (Doublet Number) following the induction of microtubule sliding in low (dark bars) and high (light bars) Ca^{2+} buffer. For microtubule sliding pattern data: *ida1* low Ca^{2+}: 3 trials, *n*=148; high Ca^{2+}: 3 trials, *n*=128; *pf3* low Ca^{2+}: 2 trials, *n*=55; high Ca^{2+}: 2 trials, *n*=56; *oda1* low Ca^{2+}: 3 trials, *n*=164; high Ca^{2+}: 3 trials, *n*=58; *pf28* low Ca^{2+}: 3 trials, *n*=113; high Ca^{2+}: 4 trials, *n*=97; *pf30pf28* low Ca^{2+}: 4 trials, *n*=107; high Ca^{2+}: 4 trials, *n*=67. For doublet number data: *ida1* low Ca^{2+}: 3 trials, *n*=115; high Ca^{2+}: 3 trials, *n*=70; *pf3* low Ca^{2+}: 2 trials, *n*=26; high Ca^{2+}: 2 trials, *n*=13.

conditions of low and high Ca^{2+} buffer; these analyses revealed major trends in microtubule sliding patterns and the identities of doublet microtubules with active dynein arms.

The results of the PCs analyses for each variable set are shown in Fig. 5 (sliding pattern) and Fig. 6 (doublet identity on the dynein exposed edge of the active area). For orientation, first consider the positions of the two wild-type strains (A54-e18 and 137c) in the microtubule sliding pattern PC ordinations (Fig. 5). Larger PC1 values have higher frequencies of sliding patterns P7 and P8 and lower frequencies of patterns P3-P6; larger values of PC2 have higher frequencies of sliding pattern P6 and lower frequencies of sliding pattern P4.

Axonemes from both wild-type strains sliding under low Ca^{2+} conditions have high frequencies of P7 and P8 sliding patterns and so have large positive values for sliding pattern PC1 (cf. Fig. 2A, Fig. 5). Under high Ca^{2+} conditions, the frequencies of the P7 and P8 sliding patterns decline and P3-P6 frequencies increase; therefore, the two wild-type strains have negative values for sliding pattern PC1 (cf. Fig. 2B and Fig. 5). The frequencies of P4 and P6 sliding patterns in axonemes from both wild-type strains were somewhat similar; this similarity is reflected in the relatively intermediate values for sliding pattern PC2 (see Figs 2 and 5).

For microtubule sliding patterns (Fig. 5), the first principal component explained 70.9% of the total variance among microtubule sliding patterns for axonemes isolated from wild-type and mutant strains in both low and high Ca^{2+} buffer. The second principal component, PC2, explained 13.9% of the total variance. Therefore, 84.8% of the information in the original data set is summarized by these two the principal components. For PCs analysis of the doublet number on the dynein exposed edge of the active area (Fig. 6), larger values for PC1 mean that there are higher frequencies of Db2 and lower frequencies of Db3 on the dynein exposed edge of the active area. Strains with larger values for PC2 have larger frequencies of Db1 and lower frequencies of Db3 on the dynein exposed edge. Under both high and low Ca^{2+} concentrations, axonemes isolated from both wild-type strains have extremely high frequencies of Db2 present on the dynein exposed edge and similar frequencies for Db1 and Db3 (Fig. 2 right panels and Fig. 6). Thus, the wild-type axonemes under both Ca^{2+} conditions have positive values for doublet number PC1 and intermediate values for doublet number PC2 (Fig. 6). PC1 for outer doublet number explained 69.5% of the total variance among axonemes isolated from wild-type and mutant strains in both low and high Ca^{2+} buffer; PC2 explained 18.6% of the total variance. Therefore, 88.1% of the information in the original data set is summarized by these two principal components.

By contrast to wild-type axonemes, those isolated from radial spoke-defective mutants slide with predominantly P7 and P8

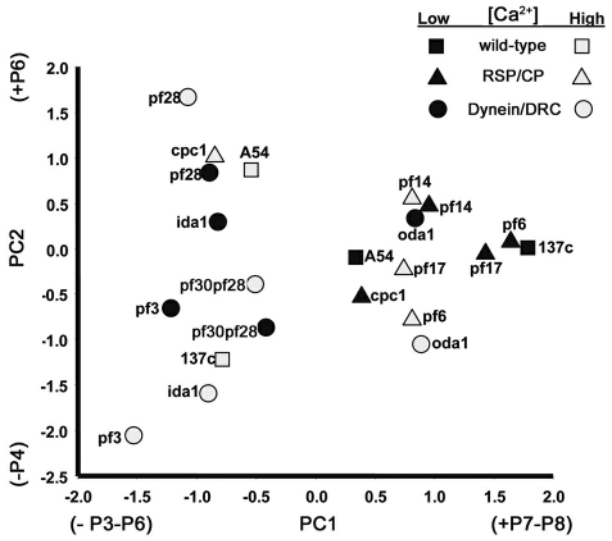

Fig. 5. Principal components analysis for microtubule sliding pattern data. The first principal component (PC1) explained 70.9% of the variation among microtubule sliding patterns for axonemes isolated from wild-type and mutant strains in both low and high Ca^{2+} buffer. Larger PC1 values have higher frequencies of sliding patterns P7 and P8 and lower frequencies of patterns P3-P6. The second principal component, PC2, explained 13.9% of the variation; larger values of PC2 have higher frequencies of sliding pattern P6 and lower frequencies of sliding pattern P4.

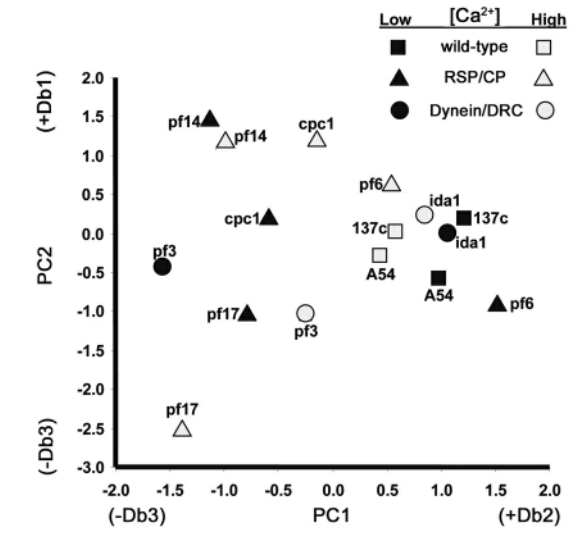

Fig. 6. Principal components analysis for data derived from the analysis of doublet number present on the dynein exposed edge of the active area. The first principal component (PC1) explained 69.5% of the variation; larger values for PC1 had higher frequencies of Db2 and lower frequencies of Db3 on the dynein exposed edge of the active area. The second principal component (PC2) explained 18.6% of the variation, with larger values for PC2 having larger frequencies of Db1 and lower frequencies of Db3 on the dynein exposed edge.

sliding patterns regardless of the Ca^{2+} condition (Figs 3 and 5). This high frequency of P7 and P8 sliding patterns is evidenced by the large positive values for PC1 in Fig. 5. The *pf14* mutant has paralyzed flagella that fail to assemble radial spokes; the *pf17* mutant has paralyzed flagella that retain the radial spoke stalks but lack the radial spoke heads (Piperno et al., 1977). Evidently, in the absence of radial spokes or spoke heads the patterns of dynein-driven microtubule sliding remain unchanged in response to increased Ca^{2+} concentration. For *pf14* axonemes the distribution of doublet microtubules present on the dynein-exposed edge is relatively random in both Ca^{2+} conditions (Figs 3 and 6). This result combined with sliding pattern data indicates that in *pf14* axonemes only one or two microtubules slide away from the axoneme, yet, microtubule sliding may occur between virtually any pair of microtubules among the nine doublets. For *pf17* axonemes, a significant percentage of transverse sections revealed that Db3 was on the dynein-exposed edge of the active area in both high and low Ca^{2+} conditions, followed by Db2 and Db4 (Figs 3 and 6). This distribution indicates that in both Ca^{2+} conditions, the dynein arms on Db2, Db3 and/or Db4 of *pf17* are the predominantly active dynein arms.

The sliding patterns of *pf6* axonemes were similar to those of radial spoke mutants; *pf6* axonemes slide with predominantly P7 and P8 patterns regardless of Ca^{2+} conditions (Figs 3 and 5). The flagella of the *pf6* mutant twitch but are unable to propel the cell; isolated *pf6* axonemes lack the 1a projection of the C1 central tubule (Dutcher et al., 1984). Evidently, in the absence of the 1a projection the axonemes fail to produce the wild-type sliding patterns associated with increased Ca^{2+} concentration. However, in stark contrast to *pf14* axonemes, microtubule sliding in *pf6* axonemes results in Db2 at the dynein-exposed edge of the active area in greater than 80% of transverse sections in low Ca^{2+} buffer and 50% of transverse sections in high Ca^{2+} buffer (Figs 3 and 6). This data combined with the predominantly P8 sliding pattern indicates that most often a single microtubule slides away from *pf6* axonemes, and this microtubule is Db3. Therefore, the dynein arms on Db2 or Db3 are the predominantly active dyneins in this mutant.

Axonemes isolated from the *cpc1* mutant are also central apparatus defective yet, produce the predominantly P8 sliding pattern in low Ca^{2+} buffer and P5 pattern in high Ca^{2+} buffer as observed for wild-type axonemes. This result may not be surprising given the motility defect in *cpc1* mutants. Flagella from *cpc1* have no obvious waveform defects, but have reduced beat frequency compared to wild-type flagella; axonemes isolated from *cpc1* lack the 1b projection of the C1 central tubule (Mitchell and Sale, 1999). For *cpc1* axonemes, Db2 was most frequently observed on the dynein-exposed edge of the active area (Figs 3 and 6). While this distribution was not random it was also not as dramatic as that seen for *pf6* or wild-type axonemes. Therefore, in the absence of the 1b projection, *cpc1* axonemes display increased variability in the outer doublet microtubules, which slide away from the axoneme, despite the fact that their sliding patterns remain relatively similar to those observed in wild-type axonemes.

Unlike the radial spoke and central apparatus-defective strains, the sliding patterns of the dynein arm mutants *pf28* (lacking outer dynein arms), *ida1* (lacking inner arm dynein I1) and *pf30pf28* (lacking I1 and outer arm dynein) as well as the dynein regulatory complex mutant *pf3*, were most similar to the patterns of sliding observed in wild-type axonemes in high Ca^{2+} buffer, regardless of the buffer conditions (Figs 4 and

5). For each of these strains, the P4, P5 and P6 patterns were the predominant microtubule sliding patterns produced in both low and high Ca^{2+} buffer. Since the flagella of strain *pf30pf28* lack both inner arm dynein subform I1 and the outer dynein arms (Piperno et al., 1990; Smith and Sale, 1992), it was not surprising that the distributions of sliding patterns for *pf30pf28* are similar to that of *ida1* and *pf28*.

For *ida1*, Db2 was on the dynein exposed edge of greater than 60% of transverse sections in both low and high Ca^{2+} buffer (Fig. 4), similar to wild-type axonemes. For *pf3* axonemes sliding in low Ca^{2+} buffer, substantial numbers of transverse sections showed Db2 on the dynein exposed edge, however, there were also significant numbers of transverse sections showing Db3 exposed (Figs 4 and 6). The number of transverse sections with Db3 exposed increased in high Ca^{2+} buffer. This increase in axonemes with Db3 exposed, as well as axonemes with additional doublets on the dynein exposed edge of the active area explains the negative doublet number PC1 and PC2 values for *pf3* axonemes sliding in either Ca^{2+} condition (Fig. 6). Since the presence of outer dynein arms is required to determine the identities of the doublets that have slid, this analysis was not possible for axonemes isolated from *pf28*, *oda1* and *pf30pf28*.

In striking contrast to *pf28*, axonemes isolated from the outer dynein arm defective mutant *oda1* slide with predominantly P7 and P8 patterns in both buffer conditions. The motility and structural defects of *pf28* and *oda1* are similar. Both strains are slow swimmers and are reported to be defective in producing the Ca^{2+}-induced change in waveform in response to photo-shock (Kamiya and Okamoto, 1985; Mitchell and Rosenbaum, 1985). Their flagella lack the outer dynein arms and beat with roughly one-half wild-type frequency. However, *oda1* also lacks the outer dynein arm docking complex proteins, which include a potential Ca^{2+} sensor (Casey et al., 2003a; Casey et al., 2003b). The results of all analyses for all strains and conditions tested are presented in tabular form in Table 2.

Discussion

Our goal was to test the idea that the axoneme possesses a control mechanism for switching active sliding between specific subsets of microtubules (Sale and Satir, 1977; Satir, 1985). Lindemann has recently proposed that the radial spokes and central apparatus play a role in modulating this switching event (Lindemann, 2003). We used an in vitro microtubule sliding assay coupled with structural analyses to determine the identities of doublet microtubules with active dynein arms in conditions of both low and high Ca^{2+} as well as in mutant axonemes lacking key axonemal components. We predicted that the in vitro assay would capture one or more phases of the beat cycle to generate non-random patterns of microtubule sliding. This prediction is based on previous analyses of microtubule sliding patterns in more intact preparations of cilia and flagella (Satir and Matsuoka, 1989). In these studies microtubule sliding patterns are modulated in response to specific experimental conditions; therefore, the in vitro assay appears to preserve certain aspects of in vivo microtubule sliding behavior.

Several conclusions can be drawn from our analyses of isolated *Chlamydomonas* axonemes. First, microtubule sliding is not random in this assay; dynein arms are active on only a subset of microtubules. As discussed below, our methods evidently induce and/or capture a single phase of the beat cycle. Second, dynein activity on specific doublet microtubules is altered in the presence of high Ca^{2+}. Finally, mutants defective in the control system do not display a wild-type response to changes in Ca^{2+}.

Dynein arms associated with a specific subset of microtubules are active

Two types of structural analyses support the conclusion that dynein arms associated with only a subset of microtubules are active. First, we analyzed the distribution of microtubule sliding patterns and discovered that this distribution is not random. Second, we took advantage of structural markers first identified in *Chlamydomonas* axonemes by Hoops and Witman (Hoops and Witman, 1983) to determine the identities of the doublet microtubules actively sliding. For wild-type axonemes, the induction of microtubule sliding in low Ca^{2+} conditions most often results in only one or two doublet microtubules sliding away from the axoneme, and these are most frequently Db3 and Db4.

Since we are unable to determine whether doublets are extruded at the plus or minus end of the axoneme, we cannot unequivocally determine whether the dynein arms on the extruded doublets are active. For example, in the simplest case where only Db3 is lacking from a transverse section, there are two possibilities for the production of the P8 sliding pattern observed in vitro. In the first case, the dynein arms on Db2 push Db3 tipward; a break occurs between Db3 and Db4 and the dynein arms on Db3 are passive. In the second scenario, the dynein arms on Db3 actively push the remaining eight doublets tipward. In this case a break occurs between Db2 and Db3 and the dynein arms on Db2 are passive. For isolated axonemes used in this assay, the minus ends of the doublet microtubules do not remain fixed; therefore, we are unable to distinguish between these two possibilities. However, in either case, it is clear that microtubule sliding is not random and occurs between a specific subset of doublet microtubules.

Based on the unique structural arrangement of microtubules in *Chlamydomonas* axonemes relative to the direction of beating (see Fig. 1), it is predicted that dynein arms on doublets Db2-Db4 generate active sliding between adjacent microtubules to produce the principal bend of the effective stroke. To produce the recovery stroke, dynein arms on doublets Db2-Db4 are predicted to switch to an inactive state, and dynein arms on doublets Db6-Db8 to switch to an active state. Given our observation that dynein arms on Db2-Db4 are most active in the in vitro sliding assay, the simplest interpretation is that we have essentially captured the equivalent of one phase of a beating flagellum, the principal bend of the effective stroke. The molecular basis for induction and/or capture of a single phase of the beat cycle is not understood.

Our previous analyses demonstrated that the C1 microtubule of the central apparatus is oriented towards the region of active microtubule sliding (Wargo and Smith, 2003). This observation combined with the data presented here indicates that C1 is oriented towards Db2-Db3. If the sliding assay captures the

Table 2. Microtubule sliding data summary

Strain		Pattern		Doublet number	
		Low Ca^{2+}	High Ca^{2+}	Low Ca^{2+}	High Ca^{2+}
Wild-type	A54-e18	P7-P8	P4-P5-P6	Db2	Db2
	137c	P7-P8	P4-P5-P6	Db2	Db2
Central pair defects	*cpc1*	P7-P8	P4-P5-P6	Db2 Db3	Db2
	pf6	P7-P8	P7-P8	Db2	Db2
Radial spoke defects	*pf14*	P7-P8	P7-P8	random	random
	pf17	P7-P8	P7-P8	Db2 Db3	Db3
DRC defect	*pf3*	P4-P5-P6	P4-P5-P6	Db3	Db2 Db3
Dynein arm defects	*ida1*	P4-P5-P6	P4-P5-P6	Db2	Db2
	oda1	P7-P8	P7-P8	n.a.	n.a.
	pf28	P4-P5-P6	P4-P5-P6	n.a.	n.a.
	pf30pf28	P4-P5-P6	P4-P5-P6	n.a.	n.a.

principal bend of the effective stroke, one prediction is that the C1 microtubule is oriented towards Db2-Db3 during the effective stroke in beating *Chlamydomonas* flagella. In recently published structural analyses of central pair orientation during flagellar beating, the C1 microtubule is oriented towards Db1 in the principal bend of the effective stroke (Mitchell, 2003), therefore, the central apparatus is oriented parallel to the plane of the bend. Given the unique technical challenges associated with examining central apparatus orientation in beating flagella and analyzing central apparatus orientation in isolated axonemes in an in vitro sliding assay, this discrepancy is remarkably small. Therefore, the structural studies of Mitchell (Mitchell, 2003) support our conclusion that the sliding assay captures the principal bend of the effective stroke.

Ca^{2+} modulates dynein activity on specific doublet microtubules

Ciliary and flagellar motility is modulated in response to changes in intraflagellar Ca^{2+}, however, the response to Ca^{2+} varies greatly between cell types. For example, in *Chlamydomonas* small increases in Ca^{2+} (pCa9-pCa7) induce a shift in flagellar dominance, differentially activating one or the other flagellum and causing the cell to photofax and turn towards light (Kamiya and Witman, 1984). A larger increase in Ca^{2+} (pCa5-pCa4) causes a momentary cessation of motility followed by a complete switch from an asymmetric to a symmetric waveform (Bessen et al., 1980). In sea urchin sperm flagella, increasing Ca^{2+} concentration increases the asymmetry of the waveform and finally induces quiescence (Brokaw, 1979; Brokaw et al., 1974; Gibbons and Gibbons, 1980). For reactivated cell models of *Paramecium* and *Tetrahymena* an increase in Ca^{2+} induces reversal of swimming direction by changing the direction of the ciliary effective stroke (Bonini et al., 1991; Hamasaki et al., 1989; Izumi, 1985; Naitoh, 1972). For each case, high Ca^{2+}-induced changes in motility are predicted to result from modulation of dynein activity on specific doublet microtubules.

Our results support this prediction. In wild-type axonemes a significantly different pattern of microtubule sliding was induced in high Ca^{2+} compared to low Ca^{2+} conditions. Following the induction of microtubule sliding, transverse sections of disrupted axonemes were most often observed with four to five doublet microtubules remaining with the central apparatus, and these microtubules were most likely to be Db7-Db2. The majority of doublets not associated with the central apparatus (Db3-Db6) were observed as individual doublets rather than clusters of four to five doublets (our unpublished observations). Therefore, either a cluster of four or five doublets slid away from the axoneme and then further dissociated into individual doublets, or individual doublets sequentially slid away from the axoneme. We are not able to distinguish between these two possibilities.

In the event that doublet microtubules have slid away from the axoneme in sequential order, there is only one explanation for the generation of the P4 or P5 sliding pattern based on the direction of force generation. Active sliding began with Db3 generating force against Db4 followed by Db4 generating force against Db5 and ending with Db6 generating force against Db7. Alternatively, if four to five doublets slid away from the axoneme as a cluster, either the dynein arms on Db2 pushed Db3-Db6 tipward with a break occurring between Db6 and Db7, or Db6 may have pushed Db7-Db2 tipward with a break occurring between Db2 and Db3. Regardless of how the P4 and P5 sliding patterns were generated, it is clear that the increased numbers of P5 and P4 sliding patterns and decrease in P8 sliding patterns is fundamentally and significantly different from the patterns observed under low Ca^{2+} conditions.

In our previous analyses we observed that the C1 microtubule of the central apparatus is also oriented towards the region of active microtubule sliding in high Ca^{2+} conditions. If the central apparatus is involved in Ca^{2+}-induced changes in waveform, it is predicted that regulatory cues provided by the central apparatus must ultimately result in modulation of sliding between specific doublet microtubules to produce changes in waveform. This prediction is supported by our observation of significant differences in the patterns of microtubule sliding in high versus low Ca^{2+} conditions. Our current analyses do not address a mechanism for Ca^{2+}-induced modulation of dynein activity. However, previous studies in *Chlamydomonas* suggest that the effect is mediated in part by calmodulin associated with the axoneme (Smith, 2002a; Yang et al., 2001). Additional Ca^{2+} binding proteins that may play a role in Ca^{2+} induced changes in motility include the Ca^{2+} binding protein centrin/caltractin (Guerra et al., 2003; Huang et al., 1988; Piperno et al., 1992; Salisbury et al., 1988; Yanagisawa and Kamiya, 2001), the 18 kDa light chain of the outer dynein arm in *Chlamydomonas* (King and Patel-King, 1995), a Ca^{2+} regulated nucleotide-diphosphate kinase in *Chlamydomonas* flagella (Patel-King et al., 2002) and the outer dynein arm docking complex protein DC3 (Casey et al., 2003a; Casey et al., 2003b).

Ca^{2+} modulation of dynein activity is defective in mutant axonemes

Substantial data have contributed to a model in which the central apparatus and radial spokes serve as signal transduction assemblies that ultimately modulate dynein activity to control the size and shape of flagellar bends (Porter and Sale, 2000). This modulation may include Ca^{2+}-induced changes in motility (Nakano et al., 2003; Smith, 2002a; Wargo and Smith, 2003; Yang et al., 2001). Our results provide additional evidence that the central apparatus and radial spokes play key roles in modulating motility in response to Ca^{2+}. The central apparatus-defective mutant *pf6* and the radial spoke-defective mutants *pf17* and *pf14* exhibit sliding patterns under both Ca^{2+} conditions that are most similar to the wild-type low Ca^{2+} sliding pattern. Evidently, these mutants are unable to respond to changes in Ca^{2+} concentration. Axonemes isolated from the *cpc1* mutant displayed wild-type sliding patterns in both Ca^{2+} conditions. This result was not surprising since the *cpc1* mutant has a wild-type photoshock response (Mitchell and Sale, 1999).

Axonemes isolated from *pf6* have a predominantly P8 sliding pattern in vitro, and remarkably, in low Ca^{2+} conditions Db3 was the doublet that slid away from the axonemes 80% of the time. We had previously shown that the C1 microtubule of the central apparatus was oriented towards the region of active sliding in *pf6* axonemes. This observation combined with the results presented here suggest that *pf6* axonemes are locked in a very specific functional conformation in which the central apparatus maintains a fixed orientation towards a single doublet, the only doublet microtubule that undergoes active sliding. Therefore, we predict that the central apparatus does not rotate in *pf6* axonemes in vivo.

The induction of microtubule sliding in *pf14* axonemes also results in a predominantly P8 sliding pattern. However, the specific doublet that slides away from the axoneme is random. We have previously shown that the C1 microtubule of the central apparatus is not oriented towards the region of active sliding in *pf14* axonemes. Taken together, these results support the conclusion that any regulatory cues ordinarily exchanged between the central apparatus and dynein arms are uncoupled in the absence of the radial spokes. These results also suggest that the orientation of the central apparatus influences dynein activity rather than dynein activity exclusively determining the orientation of the central apparatus. If dynein activity determined central pair orientation, then in spokeless mutants we would expect dynein arms to be active on the same doublet microtubules as observed for wild-type axonemes (primarily Db2-Db4), even though the central apparatus is randomly orientated in these mutants. Our results do not rule out the possibility of regulatory feedback between the radial spoke/central apparatus control system and the dynein arms.

Sliding pattern correlates with waveform

For two wild-type strains, the microtubule sliding patterns observed in high Ca^{2+} buffer were similar to those previously described for both sea urchin sperm axonemes (Nakano et al., 2003; Sale, 1986) and rat sperm axonemes (Olson and Linck, 1977) using a similar assay. Sperm flagellar axonemes beat with a symmetric waveform in low Ca^{2+} buffers; *Chlamydomonas* flagellar axonemes beat with a symmetric waveform in high Ca^{2+} buffers. These results suggest that the predicted reactivation waveform may correlate with the pattern of microtubule sliding observed in this assay. As noted, buffer conditions in which axonemes isolated from *Chlamydomonas* flagella, sea urchin sperm or rat sperm normally reactivate with a more symmetric waveform, generally produce a P5 or P4 pattern in the microtubule sliding assay. Using conditions in which *Chlamydomonas* flagella normally beat with an asymmetric waveform, isolated axonemes generally slide apart to produce a P8 or a P7 sliding pattern.

Several results support a correlation of waveform with sliding pattern. Axonemes isolated from both *pf3* and *ida1* (*pf30*) display altered waveforms when reactivated in vitro; in low Ca^{2+} buffer these mutant axonemes beat at reduced frequency with a smaller shear amplitude compared to wild-type axonemes (Brokaw and Kamiya, 1987; Kamiya et al., 1991). This reduction in shear amplitude reduces the asymmetry (increases the symmetry) of the propagating wave. Notably, axonemes isolated from both of these mutants produce sliding patterns (P5 or P4) most similar to those of wild-type axonemes in high Ca^{2+} buffer, regardless of the buffer conditions.

In addition, axonemes from the *oda1* mutants produce sliding patterns most similar to those of wild-type axonemes in low Ca^{2+} buffer, regardless of the buffer conditions. The *oda1* mutant is defective in the photoshock response in which flagellar beating switches from an asymmetric to a symmetric waveform (Kamiya, 1988). Axonemes isolated from *oda1* lack the outer dynein arms and fail to produce symmetrical waveforms in vitro using high Ca^{2+} reactivation conditions (Brokaw and Kamiya, 1987). Therefore, the sliding patterns normally produced by wild-type axonemes under high Ca^{2+} conditions are not induced in *oda1* axonemes. In contrast, the *pf28* mutant is also defective in waveform switching (Mitchell and Rosenbaum, 1985). However, axonemes isolated from *pf28* produce microtubule sliding patterns most similar to that of wild-type axonemes under high Ca^{2+} conditions, regardless of the concentration of Ca^{2+} in the buffer. Interestingly, we have previously shown that the C1 microtubule of the central apparatus is not oriented towards the region of active sliding in either *pf28* or *oda1* axonemes, indicating that in the absence of the outer dynein arms, regulatory cues produced by the central apparatus are uncoupled from microtubule sliding under high Ca^{2+} conditions (Wargo and Smith, 2003). While *pf28* axonemes lack the outer dynein arms, which is the same defect as in *oda1*, *oda1* axonemes additionally lack the outer dynein arm docking complex, which includes DC3, a Ca^{2+} sensitive binding protein (Casey et al., 2003a; Casey et al., 2003b). These results suggest a possible role for DC3 in modulating dynein-driven microtubule sliding in response to increases in Ca^{2+}.

The work was supported by NIH grant GM51379 as a consortium agreement (P. A. Lefebvre, University of Minnesota), and was supported in part by research grant 5-FY99-799 (E.F.S.) from the March of Dimes Birth Defects Foundation and the NIH grant GM66919 (E.F.S.).

References

Bessen, M., Fay, R. B. and Witman, G. B. (1980). Ca^{2+} control of waveform in isolated flagellar axonemes of *Chlamydomonas*. *J. Cell Biol.* **86**, 446-455.

Bonini, N. M., Evans, T. C., Miglietta, L. A. and Nelson, D. L. (1991). The

regulation of ciliary motility in Paramecium by Ca^{2+} and cyclic nucleotides. *Adv. Second Messenger Phosphoprotein Res.* **23**, 227-722.

Brokaw, C. J. (1979). Ca^{2+}-induced asymmetrical beating of triton-demembranated sea urchin sperm flagella. *J. Cell Biol.* **82**, 401-411.

Brokaw, C. J. (1989). Direct measurements of sliding between outer doublet microtubules in swimming sperm flagella. *Science* **243**, 1593-1596.

Brokaw, C. J., Josslin, R. and Bobrow, L. (1974). Ca^{2+} ion regulation of flagellar beat symmetry in reactivated sea urchin spermatozoa. *Biochem. Biophys. Res. Commun.* **58**, 795-800.

Brokaw, C. J. and Kamiya, R. (1987). Bending patterns of *Chlamydomonas* flagella: IV. Mutants with defects in inner and outer dynein arms indicate differences in dynein arm function. *Cell Motil. Cytoskeleton* **8**, 68-75.

Casey, D. M., Inaba, K., Pazour, G. J., Takada, S., Wakabayashi, K., Wilkerson, C. G., Kamiya, R. and Witman, G. B. (2003a). DC3, the 21-kDa subunit of the outer dynein arm-docking complex (ODA-DC), is a novel EF-hand protein important for assembly of both the outer arm and the ODA-DC. *Mol. Biol. Cell* **14**, 3650-3663.

Casey, D. M., Yagi, T., Kamiya, R. and Witman, G. B. (2003b). DC3, the smallest subunit of the *Chlamydomonas* flagellar outer dynein arm-docking complex, is a redox-sensitive Ca^{2+}-binding protein. *J. Biol. Chem.* **278,** 42652-42659.

Dutcher, S. K., Huang, B. and Luck, D. J. (1984). Genetic dissection of the central pair microtubules of the flagella of *Chlamydomonas* reinhardtii. *J. Cell Biol.* **98**, 229-236.

Fox, L. A. and Sale, W. S. (1987). Direction of force generated by the inner row of dynein arms on flagellar microtubules. *J. Cell Biol.* **105**, 1781-1787.

Gibbons, B. H. and Gibbons, I. R. (1980). Ca^{2+}-induced quiescence in reactivated sea urchin sperm. *J. Cell Biol.* **84**, 13-27.

Gorman, D. S. and Levine, R. P. (1965). Cytochrome f and plastocyanin: their sequence in the photosynthetic electron transport chain of *Chlamydomonas* reinhardtii. *Proc. Natl. Acad. Sci. USA* **54**, 1665-1669.

Guerra, C., Wada, Y., Leick, V., Bell, A. and Satir, P. (2003). Cloning, localization, and axonemal function of tetrahymena centrin. *Mol. Biol. Cell* **14**, 251-261.

Hamasaki, T., Murtaugh, T. J., Satir, B. H. and Satir, P. (1989). In vitro phosphorylation of Paramecium axonemes and permeabilized cells. *Cell Motil. Cytoskeleton* **12**, 1-11.

Harris, E. (1989). *The* Chlamydomonas *Sourcebook.* San Diego: Academic Press.

Hoops, H. J. and Witman, G. B. (1983). Outer doublet heterogeneity reveals structural polarity related to beat direction in *Chlamydomonas* flagella. *J. Cell Biol.* **97**, 902-908.

Huang, B., Piperno, G., Ramanis, Z. and Luck, D. J. (1981). Radial spokes of *Chlamydomonas* flagella: genetic analysis of assembly and function. *J. Cell Biol.* **88**, 80-88.

Huang, B., Watterson, D. M., Lee, V. D. and Schibler, M. J. (1988). Purification and characterization of a basal body-associated Ca^{2+}-binding protein. *J. Cell Biol.* **107**, 121-31.

Hyams, J. S. and Borisy, G. G. (1978). Isolated flagellar apparatus of *Chlamydomonas*: characterization of forward swimming and alteration of waveform and reversal of motion by Ca^{2+} ions in vitro. *J. Cell Sci.* **33**, 235-253.

Izumi, A., and Miki-Noumura, T. (1985). Tetrahymena cell model exhibiting Ca-dependant behavior. *Cell Motil.* **5**, 323-331.

Kamiya, R. (1988). Mutations at twelve independent loci result in absence of outer dynein arms in Chylamydomonas reinhardtii. *J. Cell Biol.* **107**, 2253-2258.

Kamiya, R. (2002). Functional diversity of axonemal dyneins as studied in *Chlamydomonas* mutants. *Int. Rev. Cytol.* **219**, 115-155.

Kamiya, R., Kurimoto, E. and Muto, E. (1991). Two types of *Chlamydomonas* flagellar mutants missing different components of inner-arm dynein. *J. Cell Biol.* **112**, 441-447.

Kamiya, R. and Okamoto, M. (1985). A mutant of *Chlamydomonas* reinhardtii that lacks the flagellar outer dynein arm but can swim. *J. Cell Sci.* **74**, 181-191.

Kamiya, R. and Witman, G. B. (1984). Submicromolar levels of Ca^{2+} control the balance of beating between the two flagella in demembranated models of *Chlamydomonas*. *J. Cell Biol.* **98**, 97-107.

King, S. M. and Patel-King, R. S. (1995). Identification of a $Ca(^{2+})$-binding light chain within *Chlamydomonas* outer arm dynein. *J. Cell Sci.* **108**, 3757-3764.

Lindemann, C. B. (2003). Structural-Functional Relationships of the Dynein, Spokes, and Central-Pair Projections Predicted from an Analysis of the Forces Acting within a Flagellum. *Biophys. J.* **84**, 4115-4126.

Mitchell, D. R. (2003). Orientation of the central pair complex during flagellar bend formation in *Chlamydomonas*. *Cell Motil. Cytoskeleton* **56**, 120-129.

Mitchell, D. R. and Rosenbaum, J. L. (1985). A motile *Chlamydomonas* flagellar mutant that lacks outer dynein arms. *J. Cell Biol.* **100**, 1228-1234.

Mitchell, D. R. and Sale, W. S. (1999). Characterization of a *Chlamydomonas* insertional mutant that disrupts flagellar central pair microtubule-associated structures. *J. Cell Biol.* **144**, 293-304.

Mohri, H., Mohri, T. and Okuno, M. (1987). Topographical relationship between the axonemal arrangement and the bend direction in starfish sperm flagella. *Cell Motil. Cytoskeleton* **8**, 76-84.

Morrison, D. F. (1990). *Multivariant Statistical Methods*. New York: McGraw-Hill.

Naitoh, Y. and Kaneko, H. (1972). Reactivated triton extracted models of Paramecium: modification of ciliary movement by Ca^{2+} ions. *Science* **176**, 523-524.

Nakano, I., Kobayashi, T., Yoshimura, M. and Shingyoji, C. (2003). Central-pair-linked regulation of microtubule sliding by Ca^{2+} in flagellar axonemes. *J. Cell Sci.* **116**, 1627-1636.

Okagaki, T. and Kamiya, R. (1986). Microtubule sliding in mutant *Chlamydomonas* axonemes devoid of outer or inner dynein arms. *J. Cell Biol.* **103**, 1895-1902.

Olson, G. E. and Linck, R. W. (1977). Observations of the structural components of flagellar axonemes and central pair microtubules from rat sperm. *J. Ultrastruct. Res.* **61**, 21-43.

Omoto, C. K. and Brokaw, C. J. (1985). Bending patterns of *Chlamydomonas* flagella: II. Ca^{2+} effects on reactivated *Chlamydomonas* flagella. *Cell Motil.* **5**, 53-60.

Omoto, C. K., Gibbons, I. R., Kamiya, R., Shingyoji, C., Takahashi, K. and Witman, G. B. (1999). Rotation of the central pair microtubules in eukaryotic flagella. *Mol. Biol. Cell* **10**, 1-4.

Patel-King, R. S., Benashski, S. E. and King, S. M. (2002). A Bipartite Ca^{2+}-regulated nucleoside-diphosphate kinase system within the *Chlamydomonas* flagellum. The regulatory subunit p72. *J. Biol. Chem.* **277**, 34271-34279.

Piperno, G., Huang, B. and Luck, D. J. (1977). Two-dimensional analysis of flagellar proteins from wild-type and paralyzed mutants of *Chlamydomonas* reinhardtii. *Proc. Natl. Acad. Sci. USA* **74**, 1600-1604.

Piperno, G., Mead, K. and Shestak, W. (1992). The inner dynein arms I2 interact with a ddynein regulatory complexd in *Chlamydomonas* flagella. *J. Cell Biol.* **118**, 1455-1463.

Piperno, G., Ramanis, Z., Smith, E. F. and Sale, W. S. (1990). Three distinct inner dynein arms in *Chlamydomonas* flagella: molecular composition and location in the axoneme. *J. Cell Biol.* **110**, 379-389.

Porter, M. E. and Sale, W. S. (2000). The 9 + 2 axoneme anchors multiple inner arm dyneins and a network of kinases and phosphatases that control motility. *J. Cell Biol.* **151**, F37-F42.

Sale, W. S. (1986). The axonemal axis and Ca^{2+}-induced asymmetry of active microtubule sliding in sea urchin sperm tails. *J. Cell Biol.* **102**, 2042-2052.

Sale, W. S. and Satir, P. (1977). Direction of active sliding of microtubules in Tetrahymena cilia. *Proc. Natl. Acad. Sci. USA* **74**, 2045-2049.

Salisbury, J. L., Baron, A. T. and Sanders, M. A. (1988). The centrin-based cytoskeleton of *Chlamydomonas* reinhardtii: distribution in interphase and mitotic cells. *J. Cell Biol.* **107**, 635-641.

Satir, P. (1968). Studies on cilia. 3. Further studies on the cilium tip and a "sliding filament" model of ciliary motility. *J. Cell Biol.* **39**, 77-94.

Satir, P. (1985). *Switching Mechanisms in the Control of Ciliary Motility*. New York: Alan R. Liss, Inc.

Satir, P. and Matsuoka, T. (1989). Splitting the ciliary axoneme: implications for a 'switch-point' model of dynein arm activity in ciliary motion. *Cell Motil. Cytoskeleton* **14**, 345-358.

Shingyoji, C., Murakami, A. and Takahashi, K. (1977). Local reactivation of Triton-extracted flagella by iontophoretic application of ATP. *Nature* **265**, 269-270.

Smith, E. F. (2002a). Regulation of flagellar dynein by Ca^{2+} and a role for an axonemal calmodulin and calmodulin-dependent kinase. *Mol. Biol. Cell* **13**, 3303-3313.

Smith, E. F. (2002b). Regulation of flagellar dynein by the axonemal central apparatus. *Cell Motil. Cytoskeleton* **52**, 33-42.

Smith, E. F. and Lefebvre, P. A. (1996). PF16 encodes a protein with armadillo repeats and localizes to a single microtubule of the central apparatus in *Chlamydomonas* flagella. *J. Cell Biol.* **132**, 359-370.

Smith, E. F. and Sale, W. S. (1992). Structural and functional reconstitution of inner dynein arms in *Chlamydomonas* flagellar axonemes. *J. Cell Biol.* **117**, 573-581.

Sokal, R. R. and Rohlf, F. J. (1995). *Biometry: The Principles and Practice of Statistics in Biological Research.* New York: W.H. Freeman and Co.

Summers, K. E. and Gibbons, I. R. (1971). Adenosine triphosphate-induced sliding of tubules in trypsin-treated flagella of sea-urchin sperm. *Proc. Natl. Acad. Sci. USA* **68**, 3092-3096.

Wargo, M. J. and Smith, E. F. (2003). Asymmetry of the central apparatus defines the location of active microtubule sliding in *Chlamydomonas* flagella. *Proc. Natl. Acad. Sci. USA* **100**, 137-142.

Witman, G. B. (1986). Isolation of *Chlamydomonas* flagella and flagellar axonemes. *Methods Enzymol.* **134**, 280-290.

Yanagisawa, H. A. and Kamiya, R. (2001). Association between actin and light chains in *Chlamydomonas* flagellar inner-arm dyneins. *Biochem. Biophys. Res. Commun.* **288**, 443-447.

Yang, P., Diener, D. R., Rosenbaum, J. L. and Sale, W. S. (2001). Localization of calmodulin and dynein light chain LC8 in flagellar radial spokes. *J. Cell Biol.* **153**, 1315-1326.

Yoshimura, M. and Shingyoji, C. (1999). Effects of the central pair apparatus on microtubule sliding velocity in sea urchin sperm flagella. *Cell Struct. Funct.* **24**, 43-54.